Multiphysics Model of Quench for the ITER Central Solenoid

(Article begins on next page)

22 December 2024

Multiphysics Model of Quench for the ITER Central Solenoid

L. Cavallucci, F. Gauthier, M. Breschi, C. Hoa, P. Bauer, A. Vostner

Abstract—**The ITER Central Solenoid (CS), the backbone of the ITER magnet system, is composed of 6 modules, each made of 40 pancakes, for a total conductor length of about 36 km. More than 4 km of pipes, about 30 bypass or control valves, the heat exchangers and a cold circulator are part of the cryogenic distribution used to maintain the nominal operating conditions (flow and temperature). During the plasma scenario, several loss sources – such as AC losses, heat from supports and structures, joule heating at joints – can affect the magnet stability. A reliable analysis of quench is therefore of great importance to guarantee the safe operation of the CS superconducting coils.**

In this work, the *SuperMagnet* code, a state of the art software for the numerical modelling of hydraulic, electrical and thermal phenomena occurring in superconducting magnets, is applied to study the CS and its cryogenic distribution during quench events.

Index Terms—**Quench, LTS, Central Solenoid, ITER, Fusion.**

I. Introduction

THE application of sophisticated numerical models [1]-[4] able to perform multi-physics analysis (thermal, hydraulic, electromagnetic) of large scale fusion magnets is important to check that adequate stability margin is available during the tokamak operations. Several numerical models were developed from the 1980s with the intent to analyse the multiphysics behaviour of a superconducting magnet: from the early works with MAGS [5] or Saruman/Gandalf [6],[7] to the most recent models with Vincenta/Venecia [8],[9], 4C code [10],[11], *SuperMagnet* [12],[13].

In this work, the *SuperMagnet* code [14] is applied to analyse the thermal-hydraulic behaviour of the CS [15]-[17] and its cryogenic loop [18],[19] during quench events occurring in critical locations. The thermal-hydraulic analysis of the CS during the $15\,\mathrm{MA}$ dynamic (DINA) plasma scenario with the *SuperMagnet* code reveals the most critical location of the magnet during its working cycle [20],[21]. The evolution of the temperature margin was investigated in the conductor for all turns of all modules and a minimum value of $1.8\,\mathrm{K}$ was observed at the end of the plasma cycle in turn #1 of the central pancakes of modules CS3L, CS1L and CS1U. This value is above the prescribed threshold of $0.7\,\mathrm{K}$ for the CS conductor.

One of these critical locations, corresponding to pancake #20 of module CS1L, is here selected to analyse the CS behaviour during quench. The CS modules currents are set

to the values corresponding to the end of the plasma cycle; no losses in the modules are taken into accounts. At the end of plasma, the magnet experiences the most critical working conditions with the lowest temperature margin. The analysis of quench in these conditions is therefore of great relevance for the magnet operation.

At the beginning of the simulation, the magnet is assumed in a "cold" state ($4.4\,\mathrm{K}$). The quench is then initiated through a $3\,\mathrm{ms}$ heat disturbance applied over the whole length of one turn. This fast perturbation allows a conservative assessment of the hot-spot temperature. Two turns of pancake #20 are selected in this study given their different characteristics:

- Turn #1 exhibits the highest field (B=12.6 T, see Fig.1), the lowest current sharing temperature (Tcs=6.3 K) and the lowest minimum quench energy.
- Turn #14 exhibit a lower field (B=0.3 T) and a higher minimum quench energy than turn #1 but, due to the higher current sharing temperature (Tcs=14.7 K), a harder quench detection is expected.

Once a quench event occurs at these locations, the intervention of the quench protection system is investigated by simulating the magnet discharge on an external resistor bank. The analysis of quench was performed with two models: the detailed *SuperMagnet* model previously adopted to study the plasma scenario, mentioned here as *closed-loop* model, and a less detailed *open-loop* model.
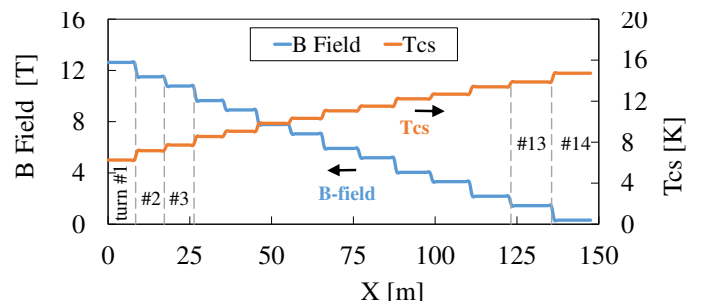
Fig. 1: Magnetic flux density (left axis) and current sharing temperature (right axis) in pancake #20 of module CS1L at the end of the plasma scenario.

II. Model Description

The *open-loop* model is characterized by a much lower computational time with respect to the *closed-loop* model. Due to this fast computation, the *open-loop* model can be applied to perform preliminary parametric studies. The results found with this model need a refinement with the detailed *closed-loop* model.

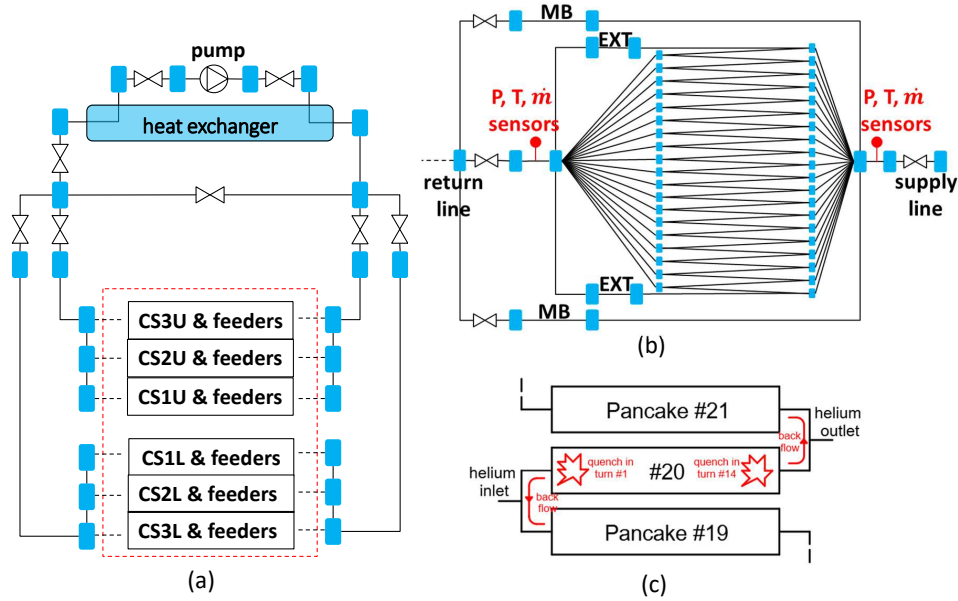Fig. 2: (a) Hydraulic scheme of the cryogenic system; (b) Module feeder and joint locations; (c) Sketch of the helium flow during quench in turn #1 and #14.

A. Closed-loop Model

In the *closed-loop* model, the same *SuperMagnet* model adopted for the analysis of the CS under the $15\,\mathrm{MA}$ plasma scenario was adopted [20],[21]. This model (Fig. 2) is able to analyse the six CS modules and their feeders with details of the cryogenic circuit through several sub-models within the *SuperMagnet* suite.

Cryogenic system and feeder: The *Flower* model [22] describes the general hydraulic loop: pipes, cryogenic pump, heat exchanger, control and by-pass valves [23],[24]. The general hydraulic scheme of one out of six modules and its feeder with details on joint location is shown in Fig. 2(b).

Pancakes model: The *Thea* model [25] is a 1-D tool for the analysis of superconducting cable that accounts for the heat conduction in the solid, the heat transfer in the coolant (bundle and spiral) and the electrical properties of the conductor [26]-[28]. The following conductors are modelled in *Thea*: CS conductors (240 in total with the characteristics of Jastec, Furukawa and Kiswire strands), lead extensions (EXT, 12 in total) and the main bus-bars (MB, 12 in total).

CS Stack model: The *Heater* model [29] is a 2-D Finite Element model describing the thermal behaviour of the CS stack (jacket, inter-turn and inter-pancake insulation, top and bottom insulation plates). *Heater* is able to model the heat diffusion between pancakes and between turns. The 2-D mesh includes nine identical equally spaced cross sections of the stack for each module. Several 1-D lines are defined to couple *Heater* to *Thea* in the frame of the *SuperMagnet* environment. The helium in connection with the jacket through these 1-D lines drives the heat exchange in azimuthal direction between the nine CS stacks. This assumption allows to implement the CS stack as nine identical 2-D cross-sections rather than as a fully 3-D stack, with a remarkable reduction of the computational burden.

B. Open-loop Model

The *open-loop* model is composed by a single process implemented in *Thea* discretizing the hydraulic and thermal characteristics of pancake #20 of module CS1L. This model neglects the effect of the thermal coupling with adjacent pancakes and also neglect the impact of the cryogenic system.

The boundary conditions are set to prescribed temperature and pressure as provided by a large (infinite) volume connected at the extremities of the pancake. These conditions impose pressure ($6.18\,\mathrm{bar}$) and temperature ($4.4\,\mathrm{K}$) of the helium entering the pancake while imposing only the pressure ($5.68\,\mathrm{bar}$) at the pancake outlet. These values are obtained by the analysis of the CS during the plasma scenario [20].
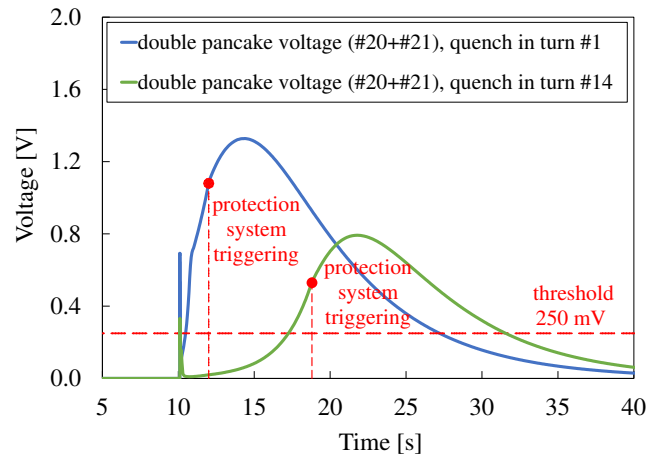

Fig. 3: Voltage profile (*closed-loop* model) registered on the double-pancake #20+#21 during a protected quench event in turn #1 and #14.
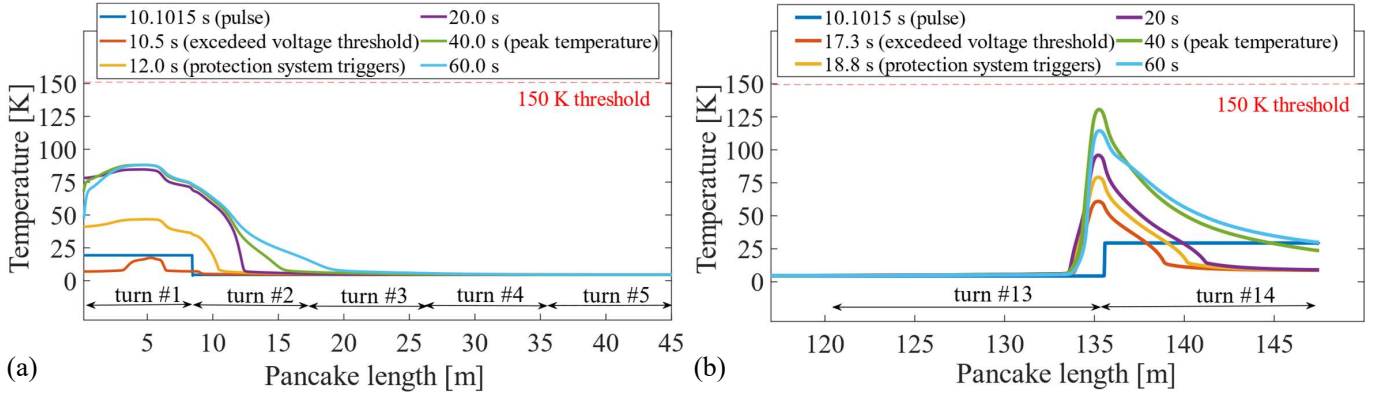
Fig. 4: Temperature profile (*closed-loop* model) in the conductor over the pancake length during quench in turn #1 (a) and #14 (b).

III. QUENCH DETECTION AND INITIALIZATION

Quench Detection: The quench detection system of the CS is based on the measurement of resistive voltage which is compared to a voltage threshold. The resistive voltage measurement is performed by the suppression of the inductive component from the voltage measurement [30]. In both the *open-loop* and the *closed-loop* models, the inductive coupling is not accounted for and the computed voltages are purely resistive. In general, the voltage across a double pancake have to be compared with the threshold value in the range from $-250\,\mathrm{mV}$ to $250\,\mathrm{mV}$. A holding time of $1.5\,\mathrm{s}$ [31] is set to check whether or not the measured voltage keeps exceeding the prescribed threshold. Once quench is triggered, the magnet is discharged with a time constant of $6.0\,\mathrm{s}$ [32]. The discharge is simulated with an exponential decay of both the current and the magnetic flux density.

Pulse Profile: To induce quench in pancake #20 of module CS1L, a $3\,\mathrm{ms}$ pulse is adopted consisting of $1\,\mathrm{ms}$ of ramp-up, $1\,\mathrm{ms}$ of flat-top and $1\,\mathrm{ms}$ of ramp-down. In both models, the pulse starts at $t = 10.1\,\mathrm{s}$. The initial phase of $10\,\mathrm{s}$ before the pulse is used to initialise the helium flow in the models.

IV. RESULTS

A. Minimum Quench Energy

Quench in Turn #1: The minimum quench energy (MQE) in turn #1 was determined increasing or decreasing the power deposited on the conductor during the pulse. A MQE of $2.44\,\mathrm{kJ}$ was computed with the *open-loop* model through a fast iterative procedure. This value was then adjusted with the *closed-loop* model and a value of $2.48\,\mathrm{kJ}$ (corresponding to $1.9\,\mathrm{J\,cm^{-3}}$) is obtained with a difference of less than $2.0\,\%$ between the two models.

Quench in Turn #14: Turn #14 is characterized by a factor 2 higher current sharing temperature and consequently a remarkable higher MQE was found: $17.7\,\mathrm{kJ}$ with the *open-loop* model and $18.44\,\mathrm{kJ}$ with the *closed-loop* one (corresponding to $9.4\,\mathrm{J\,cm^{-3}}$). Even in this turn, the MQE computed with both models exhibit a difference of about $4\,\%$.

B. Double-pancake Voltage

Quench in Turn #1: The voltage of the double pancake #20-#21 during quench in turn #1 of pancake #20 is shown in Fig. 3 (*closed-loop* model). As mentioned above, the voltage across this double-pancake is monitored by the quench protection system. At $t = 10.5\,\mathrm{s}$, the voltage exceeds the threshold of $250\,\mathrm{mV}$. After a holding time of $1.5\,\mathrm{s}$, the quench protection system intervenes and the magnet is discharged. During the discharge, a peak voltage of $1.25\,\mathrm{V}$ is reached. This value is relevant for a proper design of the inter-pancake insulation.

Quench in Turn #14: The voltage profile of the double pancake #20-#21 is also shown in Fig. 3. The voltage threshold is exceeded at $t = 17.3\,\mathrm{s}$, with a $7\,\mathrm{s}$-delay with respect to turn #1. This plays an important role on the peak temperature of this turn, as discussed in the next section. The magnet is then discharged at $t = 18.8\,\mathrm{s}$ with a lower peak voltage of $0.8\,\mathrm{V}$.

C. Temperature Profile

Quench in Turn #1: The temperature profile over the pancake length ($147.5\,\mathrm{m}$ long) is shown in Fig. 4a (*closed-loop* model). During the pulse ($t = 10.1015\,\mathrm{s}$), the temperature exhibits a rectangular shape related to the pulse profile. After the pulse, the temperature initially decreases ($t = 10.5\,\mathrm{s}$) and then rises up again and the hot zones move to the neighbouring turns. At $t = 40.0\,\mathrm{s}$, the temperature exhibits a peak of $88\,\mathrm{K}$. At $t = 60.0\,\mathrm{s}$, the peak temperature is decreasing and the hot zone is further propagating to the neighbouring turns.

Quench in Turn #14: In Fig. 4b, the temperature is shown during quench in turn#14. At $t = 40.0\,\mathrm{s}$, the temperature exhibits a peak of $137.6\,\mathrm{K}$. Despite this turn is characterized by a higher current sharing temperature than turn #1, the lower voltage during quench determines a delayed triggering of the quench protection system. This delay results in a peak temperature in turn #14 much higher than in turn #1.

It is worth noting that, despite the highest temperature in turn #14, after $30\,\mathrm{s}$ from the peak value, the temperature decreases from $137\,\mathrm{K}$ to $110\,\mathrm{K}$ while in turn #1 the peak temperature of $86\,\mathrm{K}$ remains constant for more than $70\,\mathrm{s}$ after the peak. During quench in turn #1, the temperature profile is centred on the middle of the turn while the peaked profile

observed in turn #14 is shifted towards the turn #13. In fact, in turn #1 the helium expelled during quench has the same direction of the nominal flow (from the inlet to the outlet) while, in turn #14, the expelled helium flows from the outlet to the inlet, i.e. reversed with respect to the flow imposed by the circulator.

D. Helium Flow

The helium flows differently during quench in the two turns. Even though helium expulsion is observed in both cases, the hot helium reaches different pancakes, see Fig. 2c.

Quench in Turn #1: During quench in turn #1, the expelled hot helium exits the inlet section of pancake #20 and enters pancake #19, through the common inlet manifold, thus determining a temperature increase up to $50\,\text{K}$ at the inlet of pancake #19, where no external heat disturbance is deposited.

Quench in Turn #14: During quench in turn #14, the expelled hot helium exits pancake #20 and enters pancake #21 flowing through the common outlet manifold while no hot helium enters pancake #19. A temperature increase - limited below $7\,\text{K}$ - is hence observed at the outlet of pancake #21.

E. Feeders Instrumentation

The feeders of each module are instrumented with mass flow-meters, temperature and pressure sensors located in the supply and return lines. No remarkable temperature or pressure increase is computed by the *closed-loop* model during both quench events while a different behaviour is observed for the mass-flow rate which is related to the different hydraulic configurations.

Supply line: The mass flow-meter on the supply line registers a remarkable drop of the mass-flow rate up to $50\,\%$ during quench in turn #1, see Fig. 5. The drop is instead more limited, about $14\,\%$, during quench in turn #14.

Return line: On the return line, the mass flow-meters registers an increase of $10\,\%$ during quench in turn #1 while, in case of turn #14, it increases by $55\,\%$.
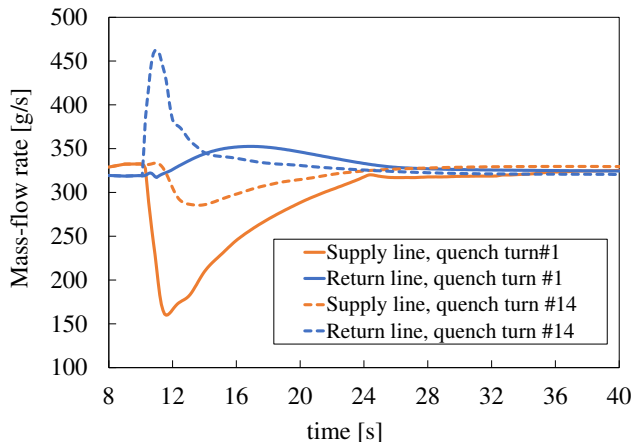

Fig. 5: Mass-flow rate profiles at the supply and return lines of the module CS1L feeder during quench in turn #1 and #14.
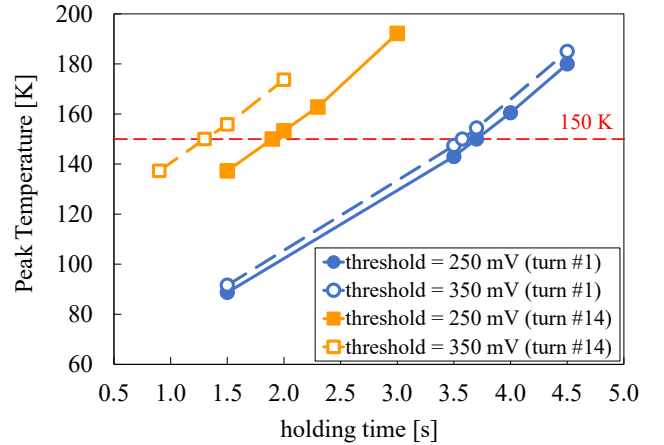

Fig. 6: Impact of the holding time on the peak temperature.

F. Impact of the holding time and voltage threshold on the peak temperature

The peak temperature during quench in turns #1 and #14 was investigated varying the two main parameters of the quench protection system: the voltage threshold and the holding time. The parametric study was performed by setting the voltage threshold to the nominal value of $250\,\text{mV}$ and to a higher value of $350\,\text{mV}$ (see Fig. 6).

According to the design requirements, a temperature threshold of $150\,\text{K}$ is prescribed on the jacket/epoxy interface. Here a conservative value of the peak temperature is assessed on the conductor. In turn #1, the temperature criterion of $150\,\text{K}$ is reached with a holding time higher than the nominal value $(1.5\,\text{s})$: $3.7\,\text{s}$ with a voltage threshold of $250\,\text{mV}$ and $3.56\,\text{s}$ with $350\,\text{mV}$. The higher temperature reached in turn #14 during quench requires a holding time closer to the nominal one. The $150\,\text{K}$-criterion is reached with a holding time of $1.9\,\text{s}$ and of $1.3\,\text{s}$ setting the voltage threshold to $250\,\text{mV}$ and $350\,\text{mV}$ respectively.

V. CONCLUSION

The analysis of quench in the CS was performed by depositing a heat disturbance over the length of turns #1 and #14 of pancake #20, module CS1L. This pancake was selected since it exhibits the lowest temperature margin during the plasma scenario. A factor 7 higher MQE was found in turn #14 than in turn #1. However turn #14 exhibits a much higher peak temperature, $10\,\text{K}$-lower than the design criteria, than turn#1.

The impact of the voltage threshold and the holding time on the peak temperature were investigated. The quench detection parameters $(250\,\text{mV},\ 1.5\,\text{s})$ are well-suited for the two very different analysed quench scenarios. In fact, in both events, a sufficient margin remains with respect to the upper prescribed limit of $150\,\text{K}$. The results in term of peak temperature versus holding time will allow quick adaptation to possible future modifications of the quench detection parameters.

REFERENCES

[1] L. Bottura, "Thermal, Hydraulic, and Electromagnetic Modeling of Superconducting Magnet Systems," *IEEE Trans. Appl. Supercond.*, vol. 26, no. 3, 2016, 4901807.

[2] A. Gavrilin, "Computer code for simulation of thermal processes during quench in superconducting magnets windings", *Cryogenics*, vol. 32, no. S1, pp. 390–393, 1992.

[3] L. Bottura, "Modelling stability in superconducting cables," *Physica* C 310, pp. 316–326, 1998.

[4] M. Bagnasco, D. Bessette, L. Bottura, C. Marinucci, and C. Rosso, "Progress in the Integrated Simulation of Thermal-Hydraulic Operation of the ITER Magnet System," *IEEE Trans. Appl. Supercond.*, vol. 20, no. 3, pp. 411-414, 2010.

[5] R. Meyder, "Investigation on effects of conductor concepts on 3D quench propagation in superconducting coils using the code system MAGS," *J. Fusion Energy*, vol. 12, no. 1/2, pp. 99–105, 1993.

[6] L. Bottura, O.C. Zienkiewicz, "SARUMAN—An integrated procedure for the analysis of quench in superconducting magnets," *IEEE Trans. Magn.*, vol. 30, no. 4, pp. 1978–1981, 1994.

[7] L. Bottura, "A Numerical Model for the Simulation of Quench in the ITER Magnets," *Journal of computational Physics*, 125, pp. 26–41, 1996.

[8] I. V. Gornikel, V. V. Kalinin, M. V. Kaparkova, V. P. Kukhtin, D. N. Shatil, N. A. Shatil, S. E. Sytchevsky, V. N. Vasiliev, "VENECIA: New Code for Simulation of Thermohydraulics in Complex Superconducting Systems" *Mathematics Information Sciences Physics*, no 3 (2), pp 127–131, 2010.

[9] alphysica http://www.alphysica.com/index.php/venecia.html

[10] L. Savoldi Richard, F. Casella, B. Fiori, R. Zanino, "The 4C code for the cryogenic circuit conductor and coil modeling in ITER," *Cryogenics* 50, pp. 167-176, 2010.

[11] R. Bonifetto, M. De Bastiani, A. Di Zenobio, L. Muzzi, S. Turtù, R. Zanino, A. Zappatore, "Analysis of the Thermal-Hydraulic Effects of a Plasma Disruption on the DTT TF Magnets," *IEEE Trans. Appl. Supercond.*, vol. 32, no. 6, 2022, 4204007.

[12] Q. Gorit, S. Nicollet, B. Lacroix, A. Louzguiti, A. Torre, F. Topin, R. Vallcorba, L. Zani, "JT-60SA TF coil quench model and Analysis: Joule energy estimation with SuperMagnet and STREAM," *Cryogenics* 124, 2022, 103454.

[13] H. Lee, S. Oh, L. Jung, "Thermo-Hydraulic Analysis of the KSTAR PF Cryogenic Loop Using SUPERMAGNET Code," *IEEE Trans. Appl. Supercond.*, vol. 28, no. 3, 2022, 4205505.

[14] CryoSoft, "SuperMagnet, Multitasking code manager", *User's Guide*, version 2.1, February 2016.

[15] N. Mitchell, D. Bessette, R. Gallix, C. Jong, J. Knaster, P. Libeyre, C. Sborchia, and F. Simon, "The ITER magnet system," *IEEE Trans. Appl. Supercond.*, vol. 18, no. 2, pp. 435-440, 2008.

[16] N.Martovetsky *et al.*, "First ITER CS module test results," *Fus. Eng. Des.*, vol. 164, 2021, 112169.

[17] T. Schild *et al.*, "Start of the ITER Central Solenoid Assembly" *IEEE Trans. Appl. Supercond.*, vol. 32, no. 6, 2008, 4202105.

[18] Hydraulic P&ID For H6 Feeder & CS3L, IDM X8Y49B.

[19] Hydraulic P&ID For H4 Feeder & CS1L, IDM YTZXF.

[20] M. Breschi, L. Cavallucci, "Support on thermal hydraulic analysis with SuperMagnet: CS loop (ACB#1) under 15 MA DT Plasma Scenario (DINA 2016-01 reference scenario)", Deliverable D1 – Contract Number IO/20/CT/4300002342, IDM 6GYCHD, Jan.2022.

[21] L. Cavallucci, F. Gauthier, M. Breschi, P. Bauer, A. Vostner, "Stability Analysis of the ITER Central Solenoid During the 15 MA DT Plasma Scenario", CHATS, oral presentation, September 2021, link available at: https://indico.iter.org/event/5/timetable/#20210922.detailed

[22] CryoSoft, "Flower, Hydraulic Network Simulation", *User's Guide*, version 4.5, January 2016.

[23] L. Bottura, C. Rosso, "Flower, a model for the analysis of hydraulic networks and processes," *Cryogenics* 43, pp. 215–223, 2003.

[24] Dong Keun Oh, "Coupled Simulation Model of CICC Components Integrated Into the Cooling Circuit" *IEEE Trans. Appl. Supercond.*, vol. 29, no. 5, 2019, 4901505.

[25] CryoSoft, "Thea, Thermal, Hydraulic and Electrical Analysis of Superconducting Cables", *User's Guide*, version 2.3, September 2016.

[26] L. Bottura, C. Rosso, M. Breschi "A general Model for thermal, hydraulic and electric analysis of superconducting cables," *Cryogenics* 40, pp. 617–626, 2000.

[27] L. Bottura, M. Breschi, A. Musso, "Calculation of interstrand coupling losses in superconducting Rutherford cables with a continuum model," *Cryogenics* 96, pp. 44-52, 2018.

[28] M. Lewandowska, A. Dembkowska, L. Zani, B. Lacroix "Thermal-Hydraulic Analysis of the DEMO PF Coils Designed by CEA," *Cryogenics* 127, 2022, 103565.

[29] CryoSoft, "Heater, Simulation of Heat Conduction", *User's Guide*, version 2.1, February 2016.

[30] Principle of Quench Detection in CS, IDM N5UYMR.

[31] DDD11-9 Instrumentation, IDM 2F2B53.

[32] M. Breschi, L. Cavallucci, P. L. Ribani, R. Bonifetto, A. Zappatore, R. Zanino, F. Gauthier, P. Bauer, N. Martovetsky, "AC losses in the first ITER CS module tests: Experimental results and comparison to analytical models," *IEEE Trans. Appl. Supercond.*, vol. 31, no. 5, 2021, 5900905.